Fabrication, microstructure and property of cellular CuAlMn shape memory alloys produced by sintering–evaporation process

S. Gong[a,b], Z. Li[a,b,*], G.Y. Xu[a], N. Liu[a], Y.Y. Zhao[c], S.Q. Liang[a]

[a] School of Materials Science and Engineering, Central south University, Changsha 410083, China
[b] Key Laboratory of Nonferrous Metal Materials Science and Engineering, Ministry of Education, Changsha 410083, China
[c] Department of Engineering, The University of Liverpool, Brownlow Hill, Liverpool L69 3GH, UK

ABSTRACT

Cellular CuAlMn shape memory alloys with open-cell or closed-cell structure have been manufactured successfully by sintering–evaporation process. This process consisted of mixing CuAlMn and NaCl powders, hot pressing and final high-temperature sintering to evaporate the filler material of NaCl powders. NaCl was eliminated completely during vacuum sintering, and strong metallurgical bonding in the cell walls was achieved. The pores' structural parameter (pore size, shape, and direction) and porosity (25–70%) have been controlled effectively. The compressing deformation behavior and phase transformation behavior of the cellular CuAlMn shape memory alloy has been investigated. It was found that the maximum stress of the cellular CuAlMn shape memory alloys increased with the decrease in porosity, and the energy absorption per unit volume approached the maximum value of 35.81 MJ/m^3 (the compression direction parallel to the cross-section) and 25.71 MJ/m^3 (the compression direction perpendicular to the cross-section) as the porosity of the alloys was 60% and the pore size was between 355 and 800 μm.

© 2010 Elsevier B.V. All rights reserved.

1. Introduction

Cellular metallic materials have attracted considerable attention in both academia and industry because of their characteristic mechanical, thermal, acoustic, electrical and chemical properties [1–15]. A variety of ways can be used to prepare the cellular metallic materials, such as self-propagating high temperature synthesis (SHS) [16,17], spark-plasma sintering (SPS) [18], infiltration process [19] or capsule-free hot isostatic pressing (CF-HIP) [20]. However, the pore structure (pore size, shape, and direction) cannot be controlled effectively using these methods. And the pore structure characteristics of the cellular metallic material have great effect on its performance. Zhao et al. [21,22] developed a sintering–dissolution process (SDP) to solve this problem. Using NaCl powder as the filler material, net-shape and open-cell Al foams with porosity in the range of 50–85% have been produced by SDP. Although other filler materials, e.g. potassium carbonate [23], urea [24] and ammonium bicarbonate [25] can also be used. NaCl powder has the outstanding advantages, such as low cost, no toxicity, no pollution, and flexible control on the NaCl particle (and thus pore) shape. However, the principal disadvantage of SDP is that it is hard

to eliminate NaCl completely from the prepared foam. In SDP [21], NaCl was removed using circulating water; the removing process may last several days, especially for large samples with small pores [26], during the long removing process, the large surfaces of the cellular metal were oxidized, and a great deal of water was being seriously wasted.

This paper develops a sintering–evaporation process (SEP) for manufacturing cellular CuAlMn shape memory alloy (SMA), which has potential applications in the fields of sound absorption and damping, especially for application in health service and medical environments, due to its low cost, high damping and inhibition of bacteria. This process can also be used to manufacture other high-melting cellular metallic materials, including Fe-, Ti- or Ni-based cellular metallic materials, the filler materials (NaCl) can be eliminated completely in the manufacturing process and no fresh water is needed to remove it. The structural characteristics and the mechanical properties of cellular CuAlMn SMAs with controlling pores' structural parameter (pore size, shape, and direction) and porosity (25–70%) produced by SEP have also been investigated.

2. Experimental procedures

2.1. Fabrication process

The raw materials used in SEP for manufacturing cellular CuAlMn alloy are CuAlMn and NaCl powders. The particle size of the NaCl powder needs to be selected according to the designed cell size of the final cellular products. In order to make sure the NaCl powders can be eliminated successfully and the pores' structural

* Corresponding author at: School of Materials Science and Engineering, Central south University, Changsha 410083, China.
Tel.: +86 731 8830264; fax: +86 731 8876692.
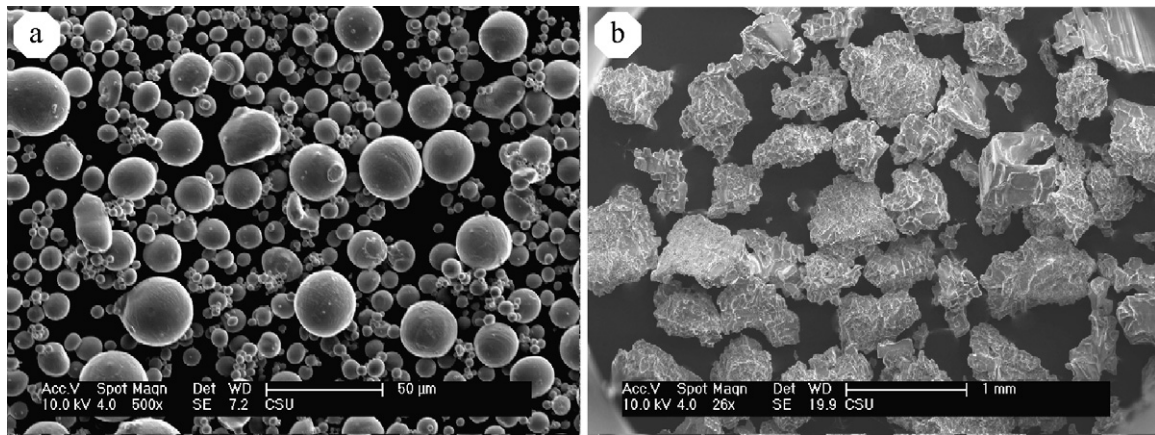E-mail address: lizhou6931@gmail.com (Z. Li).

Fig. 1. Microstructure of (a) CuAlMn powders and (b) NaCl powders (355–800 μm).

parameter can be controlled well, the particle size of the metal powder must be smaller than the NaCl powder. Pre-alloyed Cu–11.9Al–2.5Mn (wt.%) powders were produced by a liquid spraying process. The CuAlMn particles (Fig. 1a) were nearly spherical pattern and had smooth surfaces with sizes less than 75 μm. The NaCl powder (99.0% purity) had flake-like shape (Fig. 1b), and two sets of the powders (with size in the range of 355–800 μm and 800–1000 μm, respectively) were used.

The CuAlMn and NaCl powders were mixed with a weight ratio of 3:2, 2:1, 3:1, 4:1, 6:1, 10:1, respectively. A small amount of ethanol, roughly 0.5 vol% of the CuAlMn and NaCl mixture, was used as the binder during mixing. The CuAlMn and NaCl mixture was poured into a high strength graphite die and put into a vacuum furnace for hot press sintering. The sintering and evaporation procedure is illustrated in Fig. 2. The mixture was first heated to 200 °C to evaporate the ethanol and then heated to 780 °C and hot pressed at pressure of 28 MPa for 3 h with a vacuum of 0.01 Pa. After the plunger was removed, it was further heated to 930 °C for 6 h to melt and evaporate the NaCl (the melting points of NaCl and CuAlMn are 801 °C and 1040 °C, respectively), and subsequently cooled to room temperature. The compacting process used to manufacture the cellular CuAlMn is that the powders were cold compacted before vacuum sintering. The sintering neck of the final products is thinner and weaker; the strength of the final product is also lower than that prepared by vacuum hot pressing.

2.2. Characterization

The pore characteristics of the cellular CuAlMn products were analyzed using scanning electron microscopy (FEI Sirion200). The porosity of the product was obtained by the following formula [21]:

$$P = \left(1 - \frac{\rho}{\rho_0}\right) \times 100\% \tag{1}$$

where ρ and ρ_0 are the density of the cellular specimen and the density of the bulk alloy, respectively. The density of the specimen was ratio of its weight and volume. The density of the bulk Cu–11.9Al–2.5Mn (wt.%) alloy is 7.5 kg/m^3. And the volume fraction of NaCl (f_{NaCl}) in the initial CuAlMn/NaCl mixture was calculated by the following formula:

$$f_{NaCl} = \frac{\rho_0 w_{NaCl}}{\rho_0 w_{NaCl} + \rho_{NaCl} w_0} \times 100\% \tag{2}$$

where w_{NaCl} and w_0 are the weights of the NaCl powder and metal powder, respectively. Energy dispersive X-ray (EDX), X-ray diffraction analyses and weight measurement were carried out to detect the residual of NaCl in the specimen.

All the specimens were subjected to the same heat treatment (solution-treated at 800 °C for 10 min then water-quenched), all samples have martensite state. The transformation temperatures of all specimens are shown in Table 1, which were measured from differential scanning calorimetry (Perkin-Elmer DSC-7 apparatus) with a heating and cooling rate of 10 K/min under nitrogen gas protection. The mechanical behavior of the cellular CuAlMn SMA was characterized by uniaxial compression at room temperature according to ASTM standard E-9. Uniaxial compression test was carried out at a constant rate of 1 mm/min on Instron testing machine (8032-type), and the compressive stress–strain curve was recorded. The absorbed energy per unit volume, W, was defined as the area surrounded by the segment of stress–strain curve prior to the onset of densification of the sample, and it was estimated using the following relation [27]:

$$W = \int_0^{\varepsilon_D} \sigma(\varepsilon) d\varepsilon \tag{3}$$

In which, strain ε_D is defined as one at the beginning of the densification of the sample.

3. Results and discussion

3.1. Microstructure of cellular CuAlMn SMAs

The typical cell structures of the cellular CuAlMn alloy produced by SEP are shown in Fig. 3. It can be seen that the distribution of pores in all specimens is uniform. Comparing the pore morphology with that of the used NaCl powder, the pore shapes replicate the particle ones. It is demonstrated that the morphology and dimensions of the pores in the cellular CuAlMn alloy can be easily controlled by selecting an appropriate NaCl powder. A purposely tailored distribution of pore size or porosity in the cellular CuAlMn
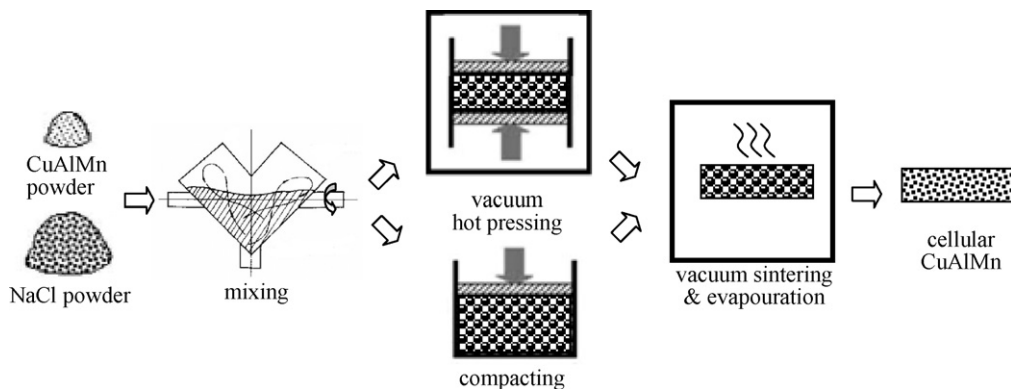

Fig. 2. Schematic of the SEP for manufacturing cellular metallic materials.

Table 1
The transformation temperatures and the energy absorption per unit volume (W) of cellular and bulk CuMnAl SMA with compression direction parallel and perpendicular to the cross-section.

Porosity (%)	Pore size (μm)	A_s (°C)	A_f (°C)	M_s (°C)	M_f (°C)	$W_{\parallel}$ (MJ/m^3)	$W_{\perp}$ (MJ/m^3)
70	800–1000	355	420	160	105	10.60	9.51
60	800–1000	366	428	134	102	19.50	16.83
60	355–800	323	439	135	104	35.81	25.71
51	355–800	320	437	125	108	29.70	17.82
45	800–1000	381	419	161	96	6.62	3.72
35	355–800	372	432	151	98	3.51	1.33
25	355–800	356	454	152	99	1.75	0.53
0	/	335	450	126	100	0.20	0.20

alloy can also be easily obtained using NaCl powders with designed particle shapes and particle size ranges.

Fig. 3c and e shows the SEM micrographs of the cross-sections of the cellular CuAlMn with a porosity of 60% and 35%, respectively. The pore sizes are in the range of 355–800 μm. High interconnecting open-cell pores are clearly shown in the former one, and closed-cell pores are uniform distributed in the latter one. Fig. 3c and d shows the SEM micrographs of the cross and longitudinal sections of the cellular CuAlMn with a porosity of 60%, respectively. On the cross-section, the pores are isometric. On the longitudinal section, however, the pores are elliptically shaped, the major axis is perpendicular to and the minor axis is parallel to the direction of the pressure applied during hot press sintering. This is due to re-arrangement of the flake like NaCl particles under pressure.

3.2. Mechanical property of cellular CuAlMn SMAs

Fig. 4 shows the compressive stress–strain curves of the cellular CuAlMn specimens produced by SEP with the porosity of 51%. The compression directions are parallel to and perpendicular to the
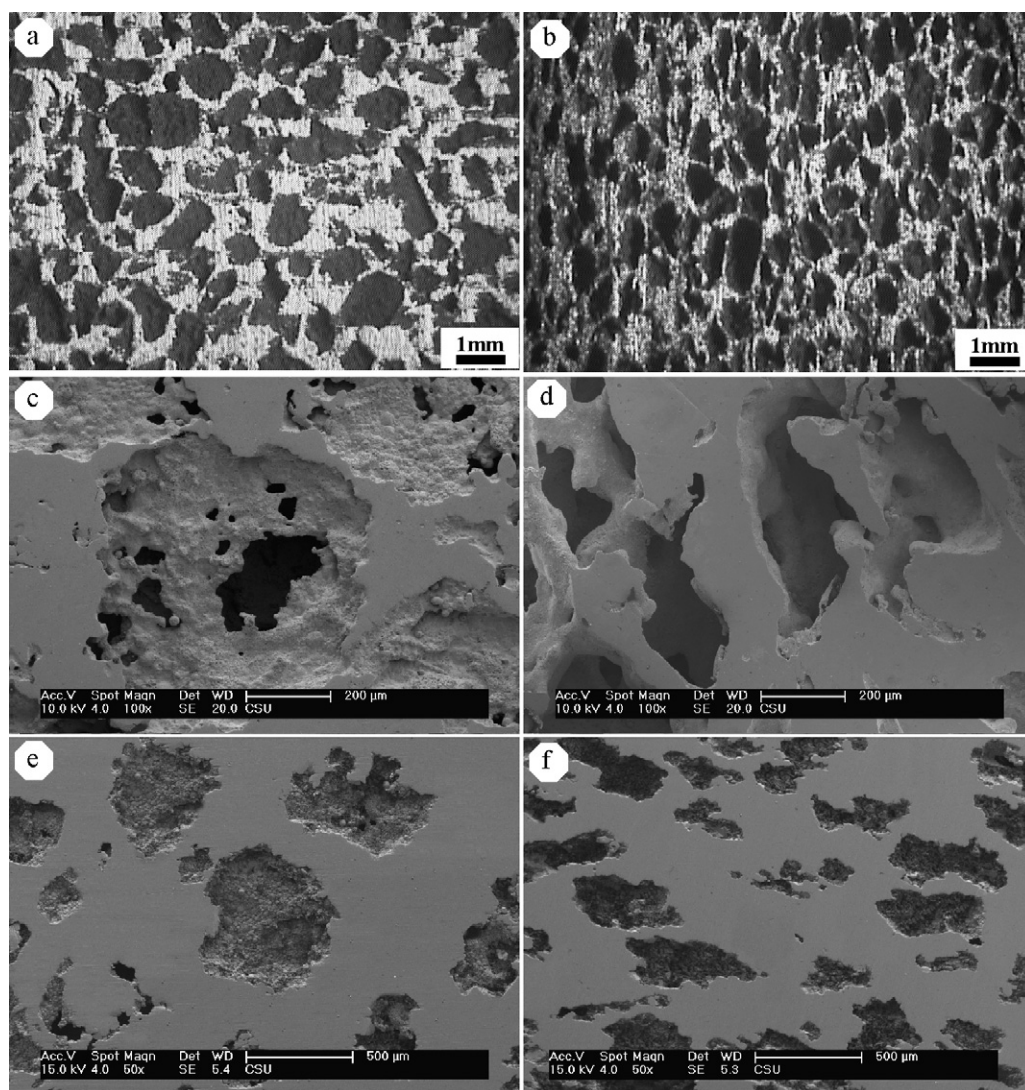

Fig. 3. Microstructure of cellular CuAlMn SMAs. (a) Optical micrograph; P = 70%; pore size: 800–1000 μm; cross-section; (b) optical micrograph; P = 70%; pore size: 800–1000 μm; longitudinal section; (c) SEM; P = 60%; pore size: 355–800 μm; cross-section; (d) SEM; P = 60%; pore size: 355–800 μm; longitudinal section; (e) SEM; P = 35%; pore size: 355–800 μm; cross-section; and (f) SEM; P = 35%; pore size: 355–800 μm; longitudinal section.

cross-section, respectively. For both cases, the evolution of compressive stress with strain shows the three regimes characteristic of cellular solids [12]: (1) Linear elasticity. At low strains, the cellular specimens deform primarily by cell-wall bending. Young's modulus is the initial slope of the stress–strain curve. (2) Plastic collapse. The plastic collapse regime has a long, flat or wave-like horizontal plateau in the stress–strain curve, indicating that plastic yielding of cell walls occurred. The plastic collapse in open-cell foams occurs when the moment exerted on the cell walls exceeds the plastic moment and plastic hinges are created. (3) Densification. When the progressive compressive plastic collapse of the cell walls proceeds to stage where the opposing cell walls meet each other and touch, most porosity has been eliminated and final densification takes place. As a consequence, the stress now rises steeply. One issue to be noted is that the stress–strain curve gained under the compression direction perpendicular to the cross-section is smoother than that gained under the compression direction parallel to the cross-section. This is due to the oriented distribution of the elliptically shaped pores in cellular CuAlMn SMAs manufactured by SEP.

During sintering, diffusion is a crucial process, which depends on the sintering time and temperature. As sintering temperature increases, sintering necks among metal particles are enlarged and reinforced, stronger metallurgical bonding is formed among the metal particles, and the strength of the pore walls enhances. If the sintering temperature is not high enough, the sintering necks among the particles are weak and the collapse in the pore walls during compression test is very likely to occur owing to the fracture of the weak sintering necks.

Besides to form the strong metallurgical bonding among the metal particles, the high temperature vacuum sintering is to eliminate the NaCl completely through the evaporation of NaCl. As the volume fraction of NaCl is more than 50%, NaCl particles contact with each other, the interconnected open-cell structure is formed after NaCl is eliminated completely. As f_{NaCl} is less than 35%, each NaCl particle is coated by metal particles (which are much smaller than NaCl particles), after NaCl is evaporated totally during vacuum sintering, sintering necks among metal particles are enlarged, the closed-cell structure is gained. The evaporation process depends on both thermodynamics and kinetics. The vapor pressure of liquid NaCl can be estimated by the following formula [28]:

$$\log 10 \left(P_v\right) = A - \left(\frac{B}{T - C}\right) \tag{4}$$

where P_v is the vapor pressure (bar) of the liquid NaCl and T is temperature (K). Between 1138 K and 1738 K, the parameter of A is 5.07184, B is 8388.497, and C is 82.638 [28]. The equilibrium

Fig. 5. Porosity dependence of maximum stress (σ) of cellular and bulk CuAlMn alloy with compression direction parallel and perpendicular to the cross-section and the volume fraction of NaCl (f_{NaCl}) in initial mixture.

vapor pressure of liquid NaCl at 1203 K (930 °C) is calculated to be 384.2 Pa, which is much higher than 0.01 Pa used in the experiments. The rate of evaporation depends on the sintering time and temperature.

Fig. 5 shows the influence of porosity, pore size and compression direction on maximum stress (σ) of cellular and bulk CuAlMn alloy and the relationship between final porosity and the volume fraction of NaCl (f_{NaCl}) in initial mixture. In order to comparison, the bulk material ($P = 0$) is also studied. σ, defined as the maximum stress on the stress–strain curve prior to the onset of densification. Porosity has a significant effect on the maximum stress of cellular CuAlMn alloy. It is revealed that the equivalent cell wall thickness is a predominant factor on the maximum stress. By decreasing the porosity from 70% to 25%, much higher maximum stress was gained in the two compression directions. The maximum stress of the sample under the compression direction parallel to the cross-section is higher than that under the compression direction perpendicular to the cross-section, which is attributed to the difference of effective stress area in two directions. The effective stress area of the sample on cross-section is smaller than that on longitudinal section owing to the oriented distribution of the elliptically shaped pores. Comparing the measured porosity with calculated f_{NaCl}, the final porosity is equivalent to the volume fraction of NaCl particles in the initial mixture, which indicates that the porosity of cellular metallic materials manufactured by SEP can be controlled effectively by selecting the weight ratio of metal and NaCl powders. In principle, cellular metallic materials with melting point higher than the melting point of NaCl (801 °C) can be manufactured by SEP. In addition to Cu-based alloy, cellular TiNi have also been manufactured.

Table 1 shows the transformation temperatures and the energy absorption per unit volume (W) of cellular and bulk CuAlMn SMA with compression direction parallel and perpendicular to the cross-section. Among all the samples, the absorbed energy of the cellular CuAlMn alloy with a porosity of 60% and pore size in the range of 355–800 μm approaches the maximum value of 35.81 MJ/m^3 and 25.71 MJ/m^3 in the two directions, respectively. W is related to the width of the flat or wave-like horizontal plateau and the stress corresponding to the plateau in the stress–strain curve. With decreasing porosity of the cellular CuAlMn alloy from 60% to 25%, the width of the horizontal plateau in the stress–strain curve decreased greatly. As a result, the energy absorption decreased accordingly in both directions. On the other side, the cellular CuAlMn alloy with porosity higher than 60% or with larger pores has much smaller stress corresponding to the plateau in the stress–strain curve, and then W also decreased.
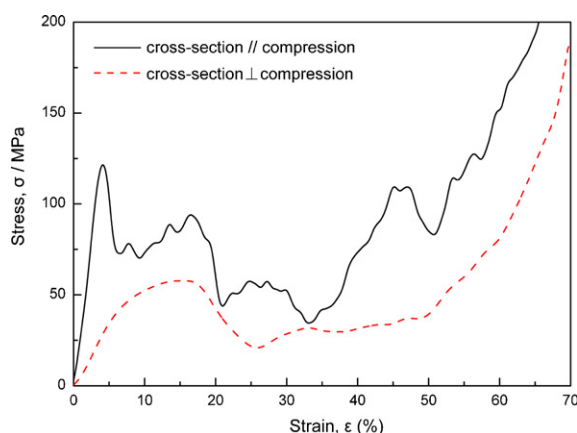

Fig. 4. Compressive stress–strain curves of cellular CuAlMn SMA with the porosity of 51%. The compression directions are parallel and perpendicular to the cross-section.
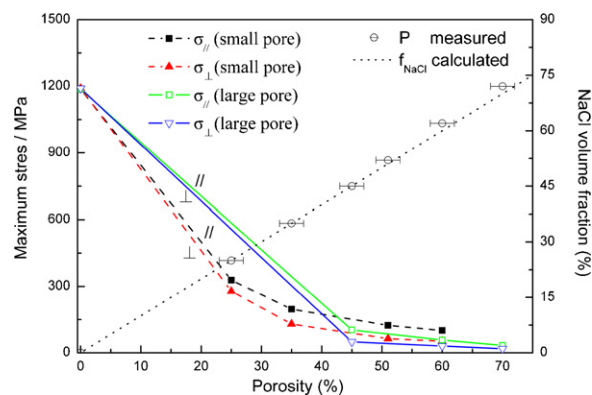
4. Conclusions

The following conclusions can be drawn from this work.

1. A novel process, sintering–evaporation process, has been developed for manufacturing cellular CuAlMn SMA, the pores' structural parameter (pore size, shape, and direction) and porosity (25–70%) can be controlled effectively.
2. Complete elimination of NaCl and strong metallurgical bonding in the cell walls of cellular CuAlMn were achieved during SEP.
3. The cellular CuAlMn SMAs with oriented distribution of the elliptically shaped pores were produced successfully by SEP. The anisotropy of the pore structure resulted in the anisotropy of mechanical properties.
4. The maximum stress on the stress–strain curve prior to the onset of densification of cellular CuAlMn SMAs increases with the decrease of porosity. And the energy absorption per unit volume reaches the maximum value of 35.81 MJ/m^3 (the compression direction parallel to the cross-section) and 25.71 MJ/m^3 (the compression direction perpendicular to the cross-section) as the porosity of the alloys was 60% and the pore size was between 355 and 800 μm.

Acknowledgments

References

[1] C.H. Wang, C.W. Luo, C.F. Huang, M.S. Huang, K.L. Ou, C.H. Yu, J. Alloys Compd. 509 (2011) 691–696.
[2] J.A. Liu, S.R. Yu, Z.Q. Hu, Y.H. Liu, X.Y. Zhu, J. Alloys Compd. 506 (2010) 620–625.
[3] E. Ergül, I. Karakaya, M. Erdogan, J. Alloys Compd. 509 (2011) 899–903.
[4] J.Y. Xiang, X.L. Wang, X.H. Xia, J. Zhong, J.P. Tu, J. Alloys Compd. 509 (2011) 157–160.
[5] Y. Liang, P. Wang, H.B. Dai, J. Alloys Compd. 491 (2010) 359–365.
[6] S. Mishraa, R. Mitra, J. Alloys Compd. 506 (2010) 308–312.
[7] N. Michailidis, F. Stergioudi, H. Omar, E. Pavlidou, D.N. Tsipas, C. Albanakis, D. Missirlis, B. Granier, J. Alloys Compd. 496 (2010) 644–649.
[8] H.L. Niu, Q. Min, Z.Y. Tao, J.M. Song, C.J. Mao, S.Y. Zhang, Q.W. Chen, J. Alloys Compd. 509 (2011) 744–747.
[9] S. Mishra, R. Mitra, M. Vijayakumar, J. Alloys Compd. 504 (2010) 76–82.
[10] A. Jinnapat, A.R. Kennedy, J. Alloys Compd. 499 (2010) 43–47.
[11] Y.F. Liu, Y.H. Cao, L. Huang, M.X. Gao, H.G. Pan, J. Alloys Compd. 509 (2011) 675–686.
[12] L.J. Gibson, M.F. Ashby, Cellular Solids: Structure and Properties, second ed., Cambridge Univ, New York, 1997.
[13] M.F. Ashby, A.G. Evans, N.A. Fleck, L.J. Gibson, J.W. Hutchinson, H.N.G. Wadley, Metal Foams: A Design Guide, Butterworth–Heinemann, Boston, 2000.
[14] J. Banhart, Prog. Mater. Sci. 46 (2001) 559–632.
[15] J. Banhart, N.A. Fleck, A. Mortensen, Cellular Metals: Manufacture, Properties and Application, MIT-Verlag, Berlin, 2003.
[16] K. Mehmet, O. Nuri, K. Bulent, K. Tahir, J. Alloys Compd. 475 (2009) 378–382.
[17] A. Moloodi, R. Raiszadeh, J. Vahdati-Khaki, A. Babakhani, J. Alloys Compd. 487 (2009) 413–419.
[18] Y. Zhao, M. Taya, Y.S. Kang, A. Kawasaki, Acta Mater. 53 (2005) 337–347.
[19] Y. Luo, S. Yu, J. Liu, X.Y. Zhu, Y.H. Luo, J. Alloys Compd. 499 (2010) 227–230.
[20] S.L. Wu, X.M. Liu, P.K. Chu, C.Y. Chung, C.L. Chu, K.W.K. Yeung, J. Alloys Compd. 449 (2008) 139–143.
[21] Y.Y. Zhao, D.X. Sun, Scr. Mater. 44 (2001) 105–110.
[22] Y.Y. Zhao, F.S. Han, T. Fung, Mater. Sci. Eng. A: Struct. Mater. Prop. Microstruct. Process. 364 (2004) 117–125.
[23] Y.Y. Zhao, T. Fung, L.P. Zhang, F.L. Zhang, Scr. Mater. 52 (2005) 295–298.
[24] D.S. Li, Y.P. Zhang, G. Eggeler, X.P. Zhang, J. Alloys Compd. 470 (2009) L1–L5.
[25] A. Laptev, M. Bram, H.P. Buchkremer, D. Stöver, Powder Metall. 47 (2004) 85–92.
[26] A. Bansiddhi, D.C. Dunand, Acta Biomater. 4 (2008) 1996–2007.
[27] U. Ramamurty, A. Paul, Acta Mater. 52 (2004) 869–876.
[28] D.R. Stull, Ind. Eng. Chem. 39 (1947) 517–550.